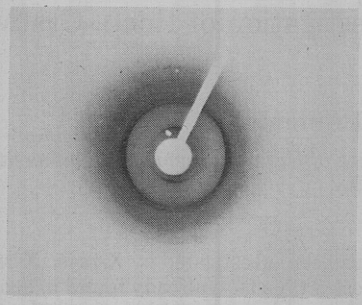

Figure 1. Normal beam X-ray diffraction pattern of *t*-Boc(L-Cys(Me))$_7$OMe oriented film; flat camera; d = 40 mm, Cu K$\bar{\alpha}$ radiation; *t*-Boc(L-Cys(Me))$_7$OMe film and stroking direction horizontal.

The c axis length is close to those found for the pentamer and hexamer of the same oligopeptide series.[10,11]

With the aid of the molecular models, we build up the antiparallel chain structure for *t*-Boc(L-Cys(Me))$_7$OMe; the peptide chain length (28 Å) is slightly shorter than the observed spacing (28.9 Å).

As far as the mode of packing of the pleated sheets is concerned, the great intensity of 200 and 001 reflections shows that all chains lie on or very near the lattice points formed by the simple cell of sides $a/2$ and c. This packing is the same already suggested by Warwicker for the silk fibroin structure.[12]

The calculated crystal density is $D_c = n0.599$ g cm^{-3}, where n is the number of peptide chains crossing the monoclinic cell. Comparison with the measured value (D_0 = 1.34 g cm^{-3}) indicates that such a cell is crossed by two β chains only. The difference between the observed and the calculated densities is undoubtedly outside the limit of the experimental error and can only be explained by the presence of solvent molecules trapped in the borderline surface of the lamellar crystallites since stringent drying conditions have not been used.

Acknowledgment. We are indebted to Professor C. Toniolo and Dr. G. M. Bonora, who kindly supplied us with the sample.

References and Notes

(1) M. Palumbo, S. Da Rin, G. M. Bonora, and C. Toniolo, *Makromol. Chem.*, **177**, 1477 (1976).
(2) C. Toniolo and M. Palumbo, *Biopolymers*, **16**, 219 (1977).
(3) J. S. Balcerski, E. S. Pysh, G. M. Bonora, and C. Toniolo, *J. Am. Chem. Soc.*, **98**, 3470 (1976).
(4) M. M. Kelly, E. S. Pysh., G. M. Bonora, and C. Toniolo, *J. Am. Chem. Soc.*, **99**, 3264 (1977).
(5) G. M. Bonora, D. Nisato, and C. Toniolo, *Makromol. Chem.*, **176**, 2535 (1975).
(6) G. M. Bonora, A. Maglione, and C. Toniolo, *Polymer*, **15**, 767 (1974).
(7) A. Elliott, R. D. B. Fraser, T. P. McRae, I. W. Stapleton, and E. Suzuki, *J. Mol. Biol.*, **9**, 10 (1964).
(8) C. Toniolo, G. M. Bonora, and A. Fontana, *Int. J. Pept. Protein Res.*, **6**, 371 (1974).
(9) R. D. B. Fraser and T. P. McRae in "Conformation in Fibrous Proteins and Related Synthetic Polypeptides", Academic Press, New York, 1973.
(10) P. Spadon, D. R. Rueda, and A. M. Piazzesi, *An. Quim.*, in press.
(11) D. R. Rueda, P. Spadon and A. Del Pra, *An. Quim.*, in press.
(12) J. O. Warwicker, *Acta Crystallogr.*, **7**, 565 (1954).
(13) *t*-Boc = *tert*-butoxy; OMe = methoxy; Cys(Me) = *S*-methylcysteine; Cys(Cbz) = *S*-carbobenzoxy-L-cysteine.

Static and Dynamical Properties of Polystyrene in *trans*-Decalin. 3. Polymer Dimensions in Dilute Solution in the Transition Region*

T. Nose‡ and B. Chu*

Department of Chemistry, State University of New York at Stony Brook, Long Island, New York 11794. *Received June 25, 1979*

ABSTRACT: Static and dynamical properties, in terms of polymer dimensions, such as the radius of gyration (r_g) and the hydrodynamic radius (r_h), and intermolecular interactions, such as the second virial coefficients (A_2, k_D, k_f), of a high molecular weight polystyrene ($M_w = 1.2 \times 10^7$) in *trans*-decalin in the dilute solution region have been investigated. We present quantitative experimental data on the temperature (T) and some molecular weight (M_w) dependence of $\bar{r}_h$ and $\langle r_g^2 \rangle_z^{1/2}$ over the transition region before the asymptotic simple power laws become valid. In the excluded volume regime for very large polymer coils dissolved in a good solvent, the blob theory of chain statistics is in very good agreement with experiments. Our data should provide experimental boundary conditions for the modification of the blob theory, even though such changes are likely to destroy the discontinuous jump from the Gaussian to the excluded volume behavior in the blob model. We also present experimental data on the contraction of polymer coils and interaction changes below the Θ temperature. Collapse of polymer coils is of interest and requires further study.

The scaling theories[1-10] have been quite successful in describing the static and dynamical properties of polymer solutions, especially in the limit $N \to \infty$, where N is the number of monomers per chain. Earlier experiments on both static properties of entangled polymer coils in the semidilute solution by small-angle neutron scattering[3] and dynamical properties of polymer (polystyrene) solutions in a good solvent (benzene) by laser light scattering[11-13] have been in reasonable agreement with predictions of the scaling laws. Furthermore, small deviations between observation and theory are often within the error limits of the experiments. However, it should be noted that with very high molecular weight polymer samples dissolved in a good solvent most reported experiments were designed

* Author to whom requests for reprints should be addressed.
‡ On leave of absence from the Department of Polymer Chemistry, Tokyo Institute of Technology.
* Work supported by the National Science Foundation and the U.S. Army Research Office.

0024-9297/79/2212-1122$01.00/0

to approach the asymptotic region of infinitely long chains where the scaling laws should hold. Consequently, agreement between theory and experiment was expected. We have no doubt that the scaling theories of polymer solutions represent a major advance in describing concentrated polymer solution behavior. In a series of publications,[14-16] we reported experiments on static and dynamical properties of a low molecular weight polystyrene (NBS 705 Standard, $M_w = 1.79 \times 10^5$, $\bar{M}_w/\bar{M}_n = 1.07$) in a poor solvent (*trans*-decalin) near (20.0 °C) the Θ temperature (20.5 °C) and at about 10 and 20 °C above the Θ temperature. By using a polymer (polystyrene) of fairly low molecular weight ($\bar{M}_w \sim 2 \times 10^5$) and by dissolving it in a Θ solvent (*trans*-decalin) where polymer coils are in a more contracted form, we expect deviations from simple scaling relations and have indeed observed gradual changes of osmotic compressibility $(\partial\pi/\partial C)_{T,P}$ as a function of concentration (C) for relatively small polymer coils instead of sharper transitions of such behavior for very large expanded coils from dilute to semidilute and concentrated solution regimes. The quantities π, C, T, and P are the osmotic pressure, the polymer concentration expressed usually in g/cm^3, the absolute temperature, and the pressure, respectively. A more significant discovery was the observation of a fast gel-like relaxation mode for polymer solutions even before the overlap concentration C^* was reached. We analyzed the measured single-clipped net signal photoelectron-count time correlation function by the histogram method[17-19] where the normalized line width distribution function $G(\Gamma)$ is represented by an equally segmented histogram in line width (Γ) space. We should mention at this point that with

$$g^{(1)}(t) = \int_0^\infty G(\Gamma) \exp(-\Gamma t)\, d\Gamma \qquad (1)$$

it is more appropriate to use variable step widths which increase exponentially with increasing Γ rather than an equally segmented step width where $g^{(1)}(t)$ is the normalized correlation function of the scattered electric field. However, the important point lies with the fact that the histogram method is completely general. It does not require an a priori assumption on the form of the line width distribution function. Consequently, we can obtain approximate quantitative information on polymer dynamics, using a correlation function profile analysis such as the histogram method. In the absence of internal segmental motions, $G(\Gamma)$ can be related to the molecular weight distribution function of a polydisperse polymer sample at zero scattering angle and infinite dilution. At finite concentrations in the dilute solution regime, $G(\Gamma)$ is influenced by intermolecular interactions, such as the second virial coefficient k_D of the translational diffusion coefficient D with

$$D = D^0(1 + k_D C + \ldots) \qquad (2)$$

At higher concentrations but before we have reached the overlap concentration

$$C = M_w/(N_A \rho_0 r_g^3) \qquad (3)$$

(where M_w, N_A, ρ_0, and r_g are the weight-average molecular weight, the Avogadro number, the solvent density, and the radius of gyration, respectively). We have observed the appearance of a new characteristic mode which is faster than the hydrodynamic diffusive mode and is responsible for the anomalous increase in the variance of the line width distribution function in the semidilute solution region. The transition from the dilute solution to the semidilute solution regime is gradual for the low molecular weight polystyrene sample ($M_w = 1.79 \times 10^5$) dissolved in *trans*-decalin. At higher concentrations where polymer coils overlap, the hydrodynamic mode becomes less important, and finally, the characteristic times responsible for the hydrodynamic mode vanish. We have identified this new mode which is faster than the hydrodynamic mode to be a pseudogel mode relating to polymer coil contact motions.

By using a low molecular weight polymer with $r_g \sim 14$ nm, we have studied mainly the Brownian motion of the center of mass of small polymer coils in the dilute solution regime and some polymer–coil overlap dynamics in the semidilute and concentrated solution regimes. We have neglected the internal mode of polymer coils because $Kr_g < 1$ where $K = (4\pi n/\lambda_0) \sin(\theta/2)$ with n, λ_0, and θ being the refractive index of the scattering medium, the wavelength of light in vacuo, and the scattering angle, respectively.

Dynamical properties including the internal modes of large polymer coils (polystyrene with M_w up to 2.4×10^7) in a good solvent (benzene) have been reported.[12,13] In this study, we want to present scattering data taken on polymer coils of very large mass ($\bar{M}_w \sim 1.2 \times 10^7$) dissolved in a Θ solvent (*trans*-decalin), measured near the Θ temperature (Θ = 20.5 °C) and up to about 20 °C above the Θ temperature. We shall divide our discussions into two parts: papers 3 and 4. The aim of paper 3 will be to provide information on the characterization of our polymer sample in the dilute solution region. In a recent paper, Akcasu and Han[20] investigated the molecular weight (M_w) and temperature dependence of the radius of gyration (r_g) and the hydrodynamic radius (r_h) of polystyrene in various solvents. They observed that under actual experimental conditions for polystyrene of finite molecular weights, the hydrodynamic radius cannot be represented by a simple power law $r_h \sim N^{\nu'}$, whereas most of the experimental data on the radius of gyration satisfy $r_g \sim N^{\nu}$ with ν' and ν being the scaling exponents. In the asymptotic region, $\nu' = \nu$. In the molecular weight range accessible experimentally, $\nu' < \nu$, as suggested by des Cloizeaux.[21] In paper 4, we shall discuss our results in the semidilute solution regime.

Definitions of Static and Dynamical Properties

1. Static Properties.[16] The osmotic compressibility has the form

$$(\partial\pi/\partial C)_{T,P} = H\,(\partial n/\partial C)_{T,P}^2 CRT/R_c(0) \qquad (4)$$

where $R_c(0)$ [$\equiv R_{vv}(0)$] is the excess Rayleigh ratio due to concentration fluctuations obtained from absolute excess scattered intensity, using vertically polarized incident and scattered light extrapolated to zero scattering angle; R is the gas constant and $H = 4\pi^2 n^2/N_A\lambda_0^4$. In dilute solution, the virial expansion has the form

$$(\partial\pi/\partial C)_{T,P} = RT/M_w + 2A_2RTC + \ldots \qquad (5)$$

where A_2 is the second virial coefficient. At finite scattering angles and concentrations, we have

$$\frac{HC}{R_{vv}} = \frac{1}{M_w}\left[1 + \frac{16\pi^2 n^2}{3\lambda_0^2}\langle r_g^2(C)\rangle_z^* \sin^2(\theta/2)\right] + 2A_2C \qquad (6)$$

where we define

$$\langle r_g^2(C)\rangle_z^* = \langle r_g^2(C)\rangle_z/(1 + 2A_2CM_w) = \frac{\text{initial slope}}{\text{intercept}}\frac{3\lambda_0^2}{16\pi^2 n^2} \qquad (7)$$

in a plot of HC/R_{vv} vs. $\sin^2(\theta/2)$ and

$$\lim_{\theta \to 0} \frac{HC}{R_{vv}} = \frac{1}{M_w} + 2A_2C \tag{8}$$

2. Dynamical Properties. The effective hydrodynamic radius r_h of the polymer is defined by

$$r_h(C) = k_BT/6\pi\eta_0D(C) \tag{9}$$

where k_B and η_0 are the Boltzmann constant and the solvent viscosity, respectively. In fact, r_h becomes appropriate only at infinite dilution where $r_h(C = 0) = k_BT/6\pi\eta_0D^0$, with D^0 being the zero concentration translational diffusion coefficient. In computing r_h, the characteristic time has to be measured essentially at small values of Kr_g ($<<1$), where the hydrodynamic translational diffusive motion dominates. Then, for a monodisperse polymer sample which exhibits a single relaxation time due to the translational motion of the center of mass of isolated polymer coils,

$$\Gamma(C = 0) = 1/\tau_0(C = 0) = D^0K^2 \tag{10}$$

where τ_0 is a characteristic decay time. For a polydisperse polymer, we define the average line width $\bar{\Gamma}$ and the second moment μ_2 as

$$\bar{\Gamma} = \int_0^\infty G(\Gamma)\Gamma \, d\Gamma \tag{11}$$

$$\mu_2 = \int_0^\infty G(\Gamma)(\Gamma - \bar{\Gamma})^2 \, d\Gamma \tag{12}$$

Then $\bar{\Gamma} = \bar{D}K^2$ and $\bar{r}_h(C = 0) = k_BT/6\pi\eta_0\bar{D}^0$.

For $Kr_g > 1$, Adam and Delsanti[12,13] have observed that, in the dilute solution region, $1/\tau_K$ increases faster than K^2, and the decay of the dynamical scattering function $S(K,t)$ is not a single exponential. The nonexponential behavior can be represented by[22]

$$S(K,t)/S(K,0) = (t\tau_K^{-1})^{2/3}\int_0^\infty du \exp[-(t\tau_K^{-1})^{2/3}u(1 + h(u))] \text{ for } t \neq 0$$

$$S(K,t)/S(K,0) = 1 \text{ for } t = 0 \tag{13}$$

where

$$h(u) = \frac{4}{\pi}\int_0^\infty \frac{dy \cos y^2}{y^3}[1 - \exp(-y^3u^{-3/2})] \tag{14}$$

with u being another variable. For polymer coils whose internal motions are within the range of photon correlation spectroscopy, the characteristic frequency

$$\tau_K^{-1} = \frac{1}{2^{3/2}3\pi}\frac{k_BT}{\eta_0}K^3 \tag{15}$$

depends only on η_0 and T. Adam and Delsanti[12,13] found that $1/\tau_K \propto K^{w+2}$ with $w + 2 = 2.85 \pm 0.05$, while the theories[22,23] predict $1/\tau_K \propto K^3$ for $Kr_g \gg 1$.

Experimental Procedures

1. **Sample Preparation.** Polystyrene was purchased from Toyo Soda Manufacturing Co. Ltd., Yamaguchi-Ken, Japan, with the following specifications: TSK Standard F-1500, $M_w = 14.7 \times 10^6$ by light scattering, $\langle r_g^2\rangle_z = 45.1 \times 10^{-11}$ cm^2 in benzene; intrinsic viscosity $[\eta]_0 = 2.96$ dL/g in *trans*-decalin at 20.4 °C; $M_w = 13.4 \times 10^6$, $M_n = 11.8 \times 10^6$ with $M_w/M_n = 1.14$ by gel permeation chromatography in methyl ethyl ketone. *trans*-Decalin was purified and filtered according to the procedure reported previously.[16] All solutions were prepared either under a dry helium atmosphere or under vacuum. We first made a 0.5 wt % polymer solution which was centrifuged at 3000–3500 g (gravitational acceleration) for 8 h. Then, we took the upper portion of the centrifuged solution as our stock solution. The condition for the centrifugation at 3000–3500 g was determined by making light scattering intensity and line width measurements of preliminary sample solutions which had been centrifuged at various rpms and over different periods of centrifugation time. We selected the condition which was sufficient to eliminate large dust particles in the solution but primarily not the large polymers themselves. Solutions at lower concentrations were prepared by dilution of a known amount of the centrifuged stock solution directly in the light scattering cell, using filtered purified *trans*-decalin. Those at higher concentrations were prepared by evaporation of the solvent from a known amount of the centrifuged stock solution in the light scattering cell, using a mild vacuum. All cells containing the solutions were flame sealed while the solutions (under vacuum) were cooled by dry ice–methanol. We prepared high molecular weight polystyrene solutions without ever using filtration. Our solution concentrations range from 0.7×10^{-4} to 3.5×10^{-2} g/g of solution.

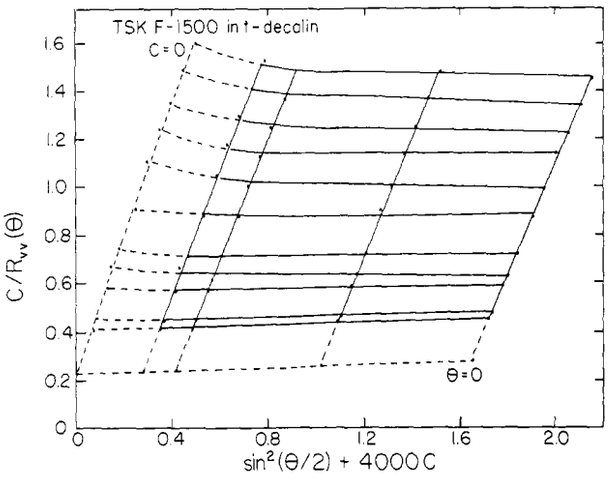

Figure 1. A Zimm plot for TSK F-1500 in *trans*-decalin at 30 °C in the dilute solution region. Note: the highest concentration (0.0415 wt % polystyrene in *trans*-decalin) is already beyond the usual dilute solution region where $(\partial\pi/\partial C)_{T,P}/T = R/M_w + 2A_2RC$ remains valid.

2. **Apparatus and Methods of Analysis.** The detailed design of the light-scattering spectrometer has been described elsewhere.[16,24,25] We used the same approach in our measurements[16] except that the polystyrene sample has a molecular weight of 12×10^6 instead of 1.79×10^5.

The measured single-clipped photocount autocorrelation function $G_k^2(t)$ $[=A(1 + \beta|g^{(1)}(t)|^2]$ is analyzed by the methods of cumulants[26] and of histogram,[17–19] where A and β are constants.

Results and Discussion

1. Static Properties. In the dilute solution region, eq 5–8 can typically be represented by a Zimm plot, as shown in Figure 1, which yields the weight average molecular weight M_w, the z-average radius of gyration $\langle r_g^2\rangle_z^{1/2}$, and second virial coefficient A_2. We obtained $M_w = 1.17 \times 10^7$ and 1.25×10^7 with NBS-705 polystyrene and benzene as our respective standard. A value of 1.2×10^7 for the weight average molecular weight is somewhat lower than those values reported by Toyo Soda. Nevertheless, we feel that the centrifugation step may have a minor effect on the final molecular weight of the polymer sample. The agreement with literature is fair. The information contained in Figure 1 is more than such a plot reveals because it does not clearly show deviations from the second virial coefficient expansion of eq 5. At temperatures below and above the Θ temperature, Figure 2 shows a plot of $(\partial\pi/\partial C)_{T,P}/T$ as a function of concentration expressed in g/g of solution. It should be noted that the concentration C in the $(\partial\pi/\partial C)_{T,P}$ term is expressed in g/cm^3. The intercept in Figure 2 corresponds to R/M_w and is equal to 7.08×10^{-7} J g^{-1} K^{-1}, yielding $M_w = 1.17 \times 10^7$ g/mol. Below the Θ temperature, a plot of $(\partial\pi/\partial C)_{T,P}$ vs. C has a slightly negative

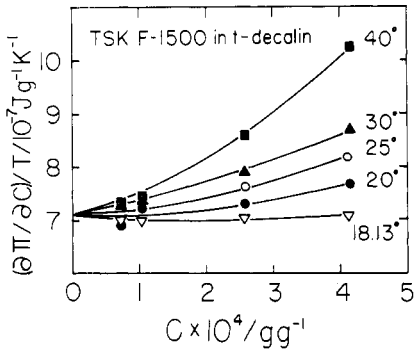

Figure 2. Plots of $(\partial\pi/\partial C)_{T,P}/T$ vs. concentration C (g/g of solution) at different temperatures in the dilute solution region. Note: the curvature of the isotherms signifies that the expression $(\partial\pi/\partial C)_{T,P}/T = R/M_w + 2A_2RC$ is valid only over very limited ranges in concentration where C is expressed in g/cm^3 except as noted.

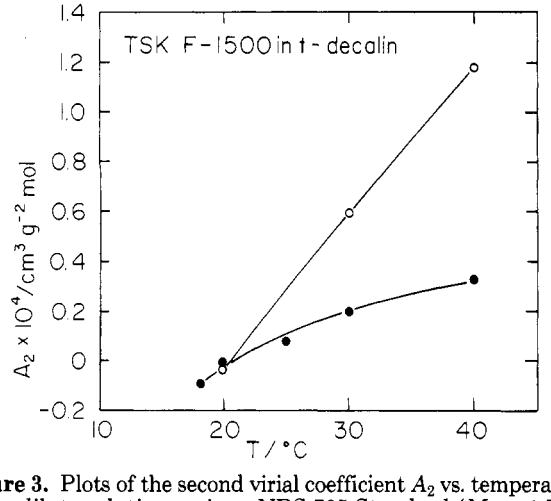

Figure 3. Plots of the second virial coefficient A_2 vs. temperature in the dilute solution region: NBS 705 Standard ($M_w = 1.79 \times 10^5$),[16] open circles; and TSK F-1500 ($M_w \sim 1.2 \times 10^7$), solid circles.

initial slope signifying a negative A_2. The curvature exists in all isotherms suggesting that the dilute solution region with only the A_2 term is valid over a very limited concentration range. The second virial coefficient A_2 has a more prominent temperature dependence for the low molecular weight polystyrene ($M_w = 1.79 \times 10^5$) than for the high molecular weight sample ($M_w \sim 1.2 \times 10^7$), as shown in Figure 3, in accordance with the data of Inagaki et al.[30] Nevertheless, A_2 becomes zero near 20.5 °C, as shown in Figure 3, for both polystyrene samples. Thus, we have reconfirmed the Θ temperature to be 20.5 °C for the polystyrene–*trans*-decalin system.

According to eq 7, we can compute an apparent radius of gyration at finite concentrations from a plot of HC/R_{vv} vs. $\sin^2(\theta/2)$. Figure 4 shows a plot of $\langle r_g^2(C)\rangle_z^{*1/2}$ vs. concentration C (g/g of solution) at different temperatures. Values of the radius of gyration extrapolated to infinite dilution are indicated in Figure 4 and replotted in Figure 5a as a function of temperature. The radius of gyration contracted from 1.75 × 10^2 nm at 40.0 °C to 9.9 × 10 nm at 17.2 °C. It appears that the rate of contraction increases with decreasing temperature, but no sharp discontinuity is observed at the Θ temperature in such a linear plot. In Figure 5b, we have plotted log $\langle r_g^2\rangle_z$ vs. log $(\Theta\tau)$ with $\tau = (T - \Theta)/\Theta$. In the Θ region, the measured exponent r with $r_g \propto \tau^{2r}$ is expected to be smaller than the predicted value of 0.2 which is valid for very high molecular weight polymers in a good solvent. In addition, we do not expect to observe a straight line behavior in Figure 5b, as the system obviously has not yet reached the asymptotic region.

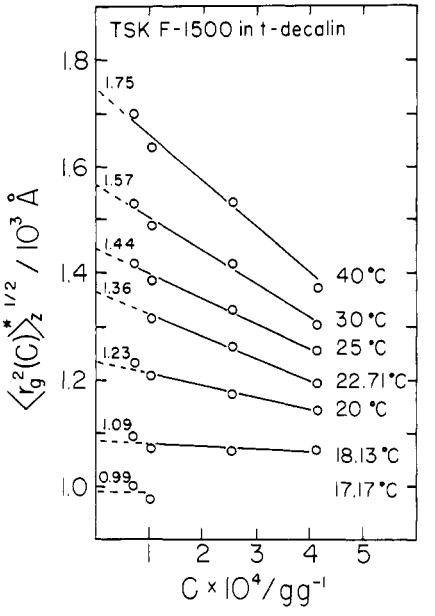

Figure 4. Plots of $\langle r_g^2(C)\rangle_z^{*1/2}$ vs. concentration C (g/g of solution) at different temperatures in the dilute solution region. $\langle r_g^2(C)\rangle_z^{*1/2}$ is defined according to eq 7.

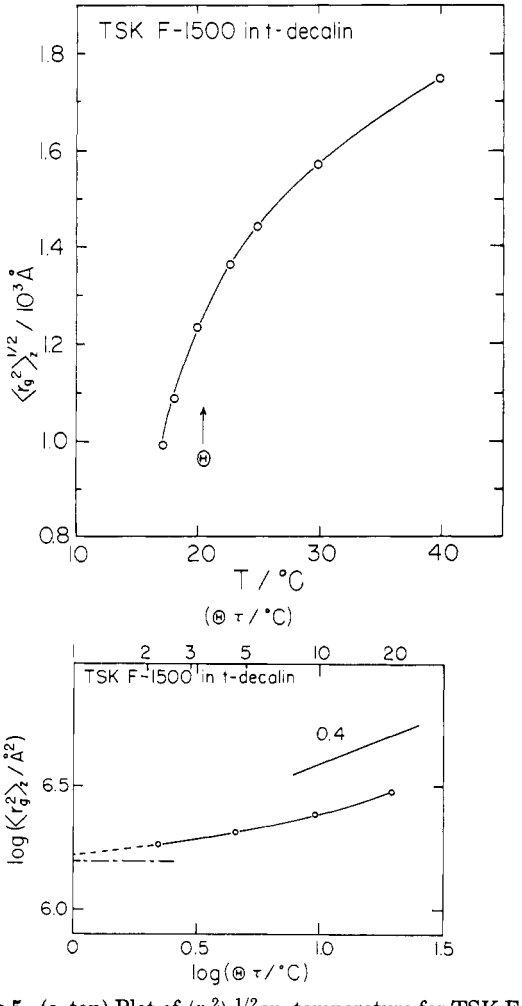

Figure 5. (a, top) Plot of $\langle r_g^2\rangle_z^{1/2}$ vs. temperature for TSK F-1500 in *trans*-decalin, Θ = 20.5 °C. (b, bottom) Log–log plot of $\langle r_g^2\rangle_z$ vs. Θτ. The dot-dash line indicated log $\langle r_g^2\rangle_z$ at $\tau = 0$. In the Gaussian regime, the measured exponent at τΘ = 20° is expected to be smaller than 0.4. $r_g^2 \sim \tau^{0.4}$ in the asymptotic limit; $\tau = (T - \Theta)/\Theta$.

Akcasu and Han[20] have investigated the molecular weight (M_w) and temperature (T) dependence of the radius

Table I
Radius of Gyration of Polystyrene in *trans*-Decalin as a Function of M_w and Temperature (Θ = 20.5 °C)

M_w, g/mol	T, °C	$\langle r_g^2\rangle_z^{1/2}$, nm	α_s[a]	N/N_τ[b]
1.79×10^5	20.0	13.0		
1.79×10^5	30.0	13.8	1.06	0.42
1.79×10^5	40.0	14.6	1.12	1.67
1.17×10^7	17.2	99	0.78	
1.17×10^7	18.1	109	0.86	
1.17×10^7	20.0	123	0.98	
1.17×10^7	20.5	126[c]	1.0	0
1.17×10^7	22.7	136	1.08	1.56
1.17×10^7	25.0	144	1.14	6.41
1.17×10^7	30.0	157	1.25	27.6
1.17×10^7	40.0	175	1.39	109

[a] $\alpha_s = \langle r_g^2\rangle_{z,T}^{1/2}/\langle r_g^2\rangle_{z,T=\Theta}^{1/2}$ with subscript T denoting temperature. [b] $N/N_\tau = M_w\tau^{*2}/416$ with $\tau^* = (T - \Theta)/T$. [c] Value obtained by interpolation.

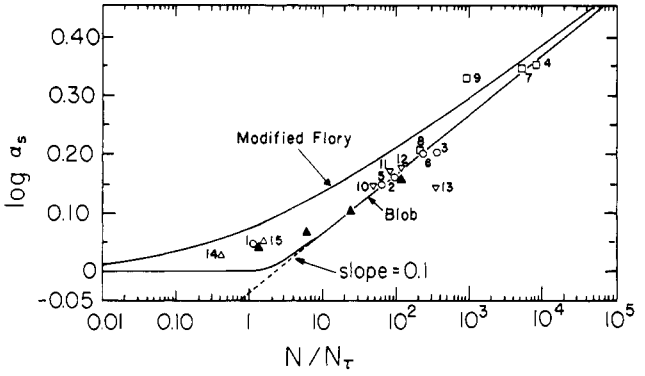

Figure 6. The variation of the expansion factor α_s for radius of gyration with $N/N_\tau = (M_w\tau^{*2}/416)$. For filled triangles, we used Θ = 20.5 °C with *trans*-decalin as solvent, $M_w = 1.17 \times 10^7$, the number of monomers in a statistical length n = 20, and the molecular weight per monomer A = 104: open triangles, polystyrene ($M_w = 1.79 \times 10^5$) in *trans*-decalin; open circles, cyclohexane; inverted open triangles, toluene; open squares, benzene. The labeled number corresponds to Table I of ref 20. The values of numbers 9 and 13 are not consistent with the others.

of gyration ($\langle r_g^2\rangle_z^{1/2}$) and the hydrodynamic radius ($\bar{r}_h$) of polystyrene in dilute solutions. By defining the linear expansion factor

$$\alpha_s = \langle r_g^2\rangle_{z,T}^{1/2}/\langle r_g^2\rangle_{z,T=\Theta}^{1/2} \tag{16}$$

they have plotted α_s as a function of N/N_τ, as shown in Figure 1 of ref 20 where $\langle r_g^2\rangle_{z,T}^{1/2}$ and $\langle r_g^2\rangle_{z,T=\Theta}^{1/2}$ are the radius of gyration at temperature T and at the Θ temperature, respectively; N now becomes the equivalent number of links (beads) in a statistical chain, and N_τ is a temperature-dependent cutoff to separate Gaussian and excluded volume regimes. The experimental points are adjusted to fit the blob theory by setting the proportionality constant α = 0.2 which yields

$$\frac{N}{N_\tau} = \frac{M_w}{416}\tau^{*2} \tag{17}$$

where we have used the number of monomers in a statistical length n = 20 and have taken $\tau^* = (T - \Theta)/T$ (instead of $\tau = (T - \Theta)/\Theta$). Table I lists values of α_s as a function of N/N_τ. We have superimposed our results of the high molecular weight polystyrene ($M_w \sim 1.2 \times 10^7$) upon those reported in Figure 1 of ref 20. The new data on polystyrene in *trans*-decalin, as shown in Figure 6, are denoted by filled triangles. They cover a range of N/N_τ from 1.56 to 109, where there are virtually no experimental points. Furthermore, our measurements concentrate on

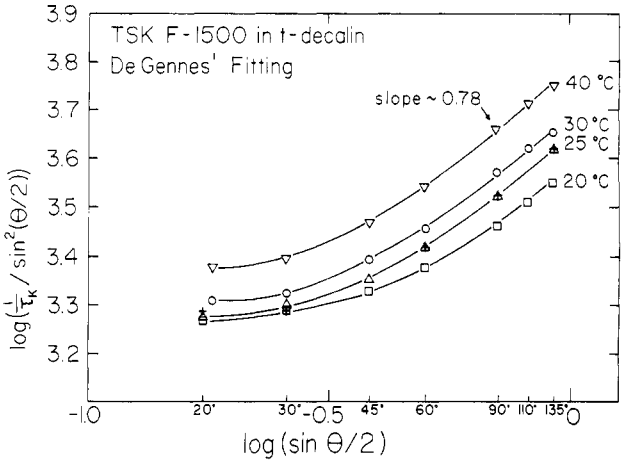

Figure 7. Log–log plots of $(1/\tau_K)\sin^2(\theta/2)$ vs. $\sin(\theta/2)$ according to eq 13 and 14 at $C = 2.57 \times 10^{-4}$ g/g of solution (open symbols) and $C = 1.06 \times 10^{-4}$ g/g of solution (crosses).

the transition behavior ($N/N_\tau \sim 1$) of α_s from the nonasymptotic region to the asymptotic region where $N/N_\tau \gg 1$. α_s exhibits a slower approach to the asymptotic behavior than the blob theory does and follows the shape of the modified Flory theory.

2. Dynamical Properties. In dilute solutions, we observe the Brownian motion of the whole macromolecule when $Kr_g \ll 1$. The line width is related to the translational diffusion coefficient by means of eq 10, and we can compute the hydrodynamic radius according to eq 9 provided that the Stokes–Einstein relation holds. At $Kr_g > 1$, the dynamical scattering function $S(K,t)$ reflects properties of the polymer chain on distances smaller than r_g. However, we can still take

$$D = (1/\tau_K)K^2 = k_BT/6\pi\eta_0L \tag{9a}$$

by assuming the validity of the Stokes–Einstein relation where L is a characteristic length of the system. By using eq 13 and 14 to analyze the nonexponential time correlation function behavior of our high molecular weight polystyrene ($M_w \sim 1.2 \times 10^7$) in *trans*-decalin, we have observed the theoretical prediction[22] that the dynamical structure factor $S(K,t)$ varies continuously with K. Figure 7 shows log–log plots of $(1/\tau_K)\sin^2(\theta/2)$ vs. $\sin(\theta/2)$, according to eq 13 and 14, at $C = 2.57 \times 10^{-4}$ g/g of solution (open symbols) and $C = 1.06 \times 10^{-4}$ g/g of solution (crosses). At small values of K, where $\theta \approx 20°$, we observed essentially $1/\tau_K = D(K)K^2$, where the diffusion coefficient $D(K)$ may be interpreted as the hydrodynamic motion of a portion of the polymer chain within a wavelength of momentum transfer, not necessarily the translational motion of the entire molecule. At $Kr_g \ll 1$, $D(K)$ involves the entire molecule so that $S(K,t)$ has an exponential form for a monodisperse polymer system and $D(K)$ reduces to D as defined by eq 10. At higher scattering angles, the characteristic time behaves as

$$\tau_K^{-1} \propto K^\gamma \tag{18}$$

with γ = 2.78, which is somewhat lower than the value of 2.85 ± 0.05 as reported by Adam and Delsanti.[12,13] However, the discrepancy is quite understandable, as Figure 7 clearly shows a continuous variation of the dynamical structure factor $S(K,t)$ from K^2 to K^3. We have not yet reached the asympototic region of K^3; neither have Adams and Delsanti. Figure 8 shows plots of $\eta_0/(\tau_K K^2 T)$ vs. K (for the same measurements as in Figure 7) at various temperatures. We have indicated the scales of $K\langle r_g^2\rangle_z^{1/2}$ at 20, 30, and 40 °C and have compensated for the changes

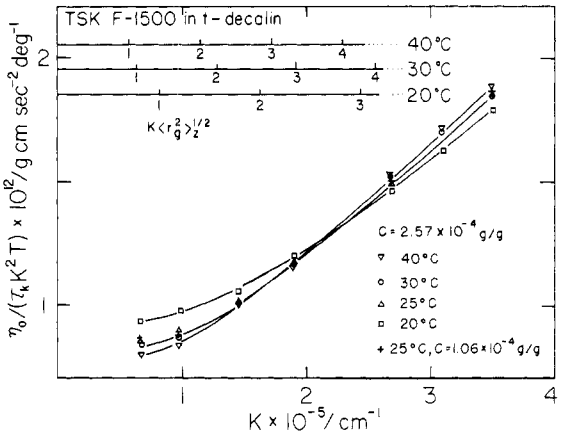

Figure 8. Plots of $\eta_0/(\tau_K K^2 T)$ vs. K with $K\langle r_g^2\rangle_z^{1/2}$ scales at $C = 2.57 \times 10^{-4}$ g/g of solution (open symbols) and $C = 1.06 \times 10^{-4}$ g/g of solution (crosses).

of τ_K^{-1} in viscosity and temperature as suggested by eq 9a and 15. At higher temperatures, such as 40 °C, the polymer coil is more expanded. Thus, over the same K range, we observe a value of γ closer to 3. At lower temperatures, such as those of 20 and 25 °C, we note that $\eta_0/(\tau_K K^2 T)$ approaches a relatively constant value near $Kr_g \sim 1$, while the same quantity at 40 °C approaches a relatively constant value at a smaller value of K where $Kr_g \sim 1$.

In our data analysis, we have tried to obtain the translational diffusion coefficient D by extrapolation of $\eta_0\bar{\Gamma}/K^2$, using different orders of cumulants fit obtained at increasingly smaller scattering angles. Unfortunately, experimental conditions have prevented us from making definitive light-beating measurements below $\theta = 20°$. Thus, we have force fitted the nonexponential form of the time correlation function, using cumulants expansion up to fifth order where the normalized time correlation of the scattered electric field has the form

$$|g^{(1)}(t)| = \exp(-\bar{\Gamma}t)(1 + \mu_2 t^2/2! - \mu_3 t^3/3! + \ldots) \qquad (19)$$

with t up to the fifth power. At higher values of $K\langle r_g^2\rangle_z^{1/2}$ (>1), the time correlation function deviates more from the single exponential behavior even for a monodisperse polymer system. Consequently, different order cumulants tend to have the apparent $\bar{\Gamma}$ values differing from one another, as shown typically in Figure 9. As $K\langle r_g^2\rangle_z^{1/2}$ becomes smaller ($\lesssim 1$), $D(K)$ approaches the translational diffusion coefficient of the entire coil, the time correlation function of a relatively narrow molecular weight distribution polymer becomes more single exponential in form, and the apparent $\bar{\Gamma}$, using different order cumulants fit, approaches the value of the second-order fit. We estimated the correct value of $\bar{\Gamma}$ by extrapolating the $\eta_0\bar{\Gamma}/K^2$ values to $K\langle r_g^2\rangle_z^{1/2} = 0$. At 17.2, 18.1, and 20.0 °C, we obtained respectively

$$\lim_{K\langle r_g^2\rangle_z^{1/2}\to 0} \frac{\eta_0\bar{\Gamma}}{K^2} = 3.31 \times 10^{-10},\ 3.10 \times 10^{-10},\ \text{and}\ 2.85 \times 10^{-10}\ \text{erg cm}^{-1}$$

By the above procedure, we determined at various temperatures and concentrations

$$\bar{D}(C) = \left(\lim_{K\langle r_g^2\rangle_z^{1/2}\to 0} \frac{\eta_0\bar{\Gamma}(C)}{K^2}\right)\frac{1}{\eta_0} \qquad (20)$$

representing the translational diffusion coefficient of the entire coil at a fixed temperature and concentration. Figure 10 shows plots of $\bar{r}_h(C) = k_B T/6\pi\eta_0\bar{D}(C)$ vs. concentration. The temperature dependence of k_D, as defined by eq 2, is related to the temperature dependence of the second virial coefficient A_2. We again found k_D to be negative below the Θ temperature. k_D became increasingly more positive at larger positive temperature distances beyond the Θ temperature. The values of $\bar{r}_h(C = 0)$, as defined by $\bar{r}_h = k_B T/6\pi\eta_0\bar{D}^0$, are listed in Table II. Figure 11 shows a plot of $\bar{r}_h$ as a function of temperature. It is especially interesting to note the sharper drop in the hydrodynamic size at temperatures below the Θ temperature. Similarly, the radius of gyration as well as the linear expansion factor of the radius of gyration α_s decreases as a function of temperature, but the rate is sharper below the Θ temperature. Figure 12 shows the variation of the expansion factor α_h for the hydrodynamic radius with N/N_r. Again we have superimposed our experimental data on Figure 3 of ref 20. By using two different molecular weights of polystyrene ($M_w = 1.79 \times 10^5$ and 1.17×10^7)

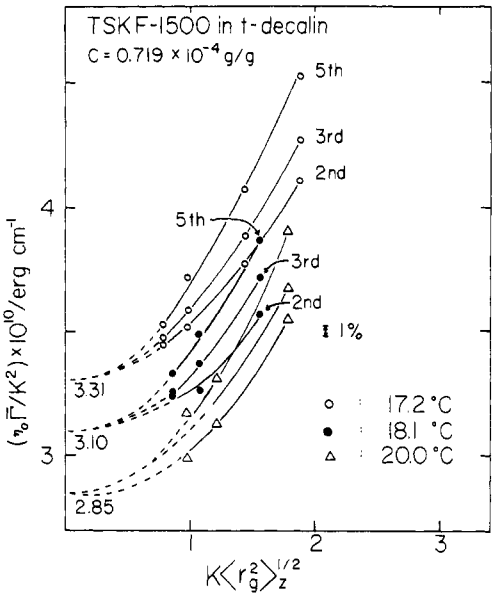

Figure 9. Typical plots of $\eta_0\bar{\Gamma}/K^2$ vs. $K\langle r_g^2\rangle_z^{1/2}$ at 17.2, 18.1, and 20.0 °C. The apparent average line width $\bar{\Gamma}$ is obtained by force fitting the net time correlation function $|g^{(1)}(\tau)|$, using the different order cumulants fit. By extrapolating $\bar{\Gamma}$ to $K = 0$, we obtain $\bar{D}$ ($=\bar{\Gamma}/K^2$), which is the translational diffusion coefficient of the entire polymer coil at a finite concentration C.

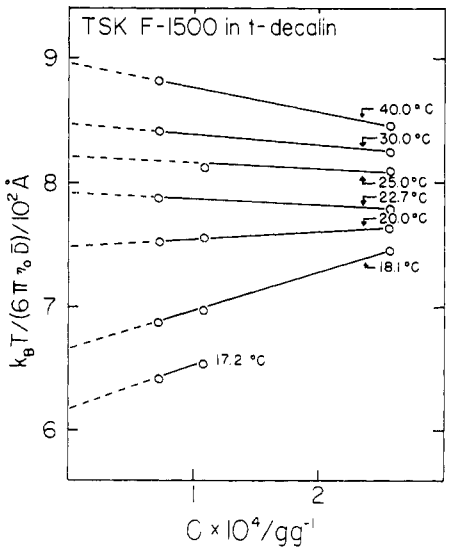

Figure 10. Plots of $k_B T/6\pi\eta_0\bar{D}$ vs. C (g/g of solution) at different temperatures. Values of $\bar{r}_h = \lim_{C\to 0} k_B T/6\pi\eta_0\bar{D}$ are listed in Table II.

Table II
Hydrodynamic Radius $\bar{r}_h$ of Polystyrene in *trans*-Decalin as a Function of M_w and Temperature (Θ = 20.5 °C)

M_w, g/mol	T, °C	$\bar{r}_h$, nm[a]	α_h[b]	$\bar{r}_h/\langle r_g^2\rangle_z^{1/2}$	α_h/α_s
1.79×10^5	20.0	9.11		0.700	
1.79×10^5	30.0	9.39	1.03	0.680	0.971
1.79×10^5	40.0	9.68	1.06	0.663	0.946
1.17×10^7	17.2	62	0.82	0.63	1.05
1.17×10^7	18.1	67	0.88	0.62	1.02
1.17×10^7	20.0	75	0.99	0.61	1.01
1.17×10^7	20.5	76[c]	1.00	0.60	1.00
1.17×10^7	22.7	79	1.04	0.58	0.963
1.17×10^7	25.0	82	1.08	0.57	0.947
1.17×10^7	30.0	85	1.12	0.54	0.896
1.17×10^7	40.0	90	1.18	0.51	0.849

[a] $\bar{r}_h = \lim_{C\to 0} k_B T/6\pi\eta_0 \bar{D}$. [b] $\alpha_h = \bar{r}_{h,T}/\bar{r}_{h,T=\Theta}$ with subscript T denoting temperature. [c] Value obtained by interpolation.

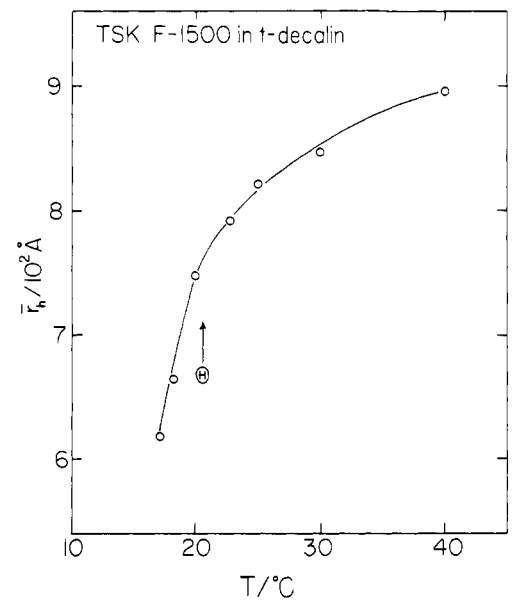

Figure 11. Variation of the hydrodynamic radius $\bar{r}_h$ as a function of temperature above and below the Θ temperature.

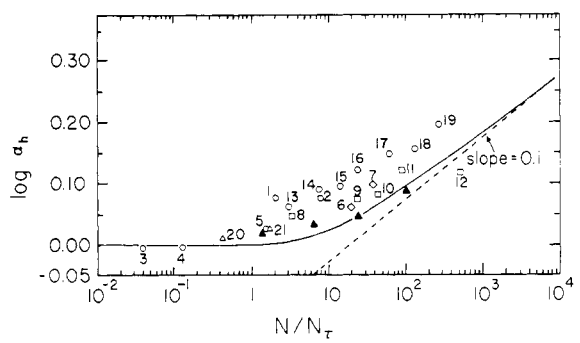

Figure 12. The variation of the expansion factor α_h for the hydrodynamic radius with $N/N_\tau = (M_w\tau^{*2}/416)$. We used the same values as those used in Figure 6. The triangles represent our data in *trans*-decalin as listed in Table II: open triangles, $M_w = 1.79 \times 10^5$; filled triangles, $M_w = 1.17 \times 10^7$; open circles, cyclohexane; open diamonds, toluene; open squares, benzene; open hexagons, THF. The labeled number corresponds to Table II of ref 20.

and *trans*-decalin, we were able to extend the ranges of N/N_τ over the transition range from the nonasymptotic region to the region where simple power laws are obeyed. Thus, in the present context, it is again not appropriate to represent our experimental data in terms of power laws.

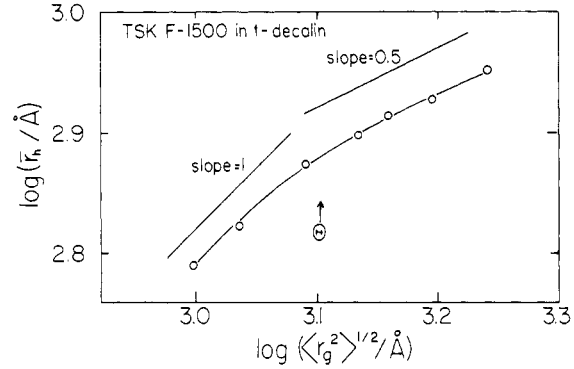

Figure 13. Log–log plot of $\bar{r}_h$ vs. $\langle r_g^2\rangle_z^{1/2}$. The slopes as shown suggest the relative change in the rate of contraction with decreasing temperature for the hydrodynamic radius and the radius of gyration.

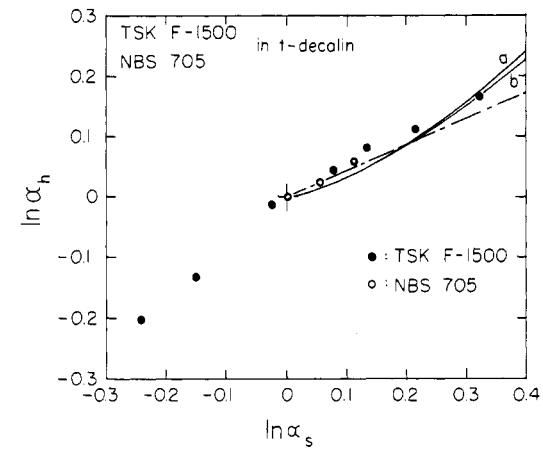

Figure 14. Ln–ln plot of α_h vs. α_s. Solid lines were calculated by eq 21 and 22, using $\nu = 0.59$ (a)$_3$ and $^3/_5$ (b)$_3$. Dot-dash line: $\alpha_\eta^3 = \alpha_s^{2.43}$ with $\alpha_\eta^3 = \alpha_s^2\alpha_h$.

We show that, in the high N/N_τ range, the blob theory is very good. In Table II, we have noted that the ratio of the hydrodynamic radius to the radius of gyration $\bar{r}_h/\langle r_g^2\rangle_z^{1/2}$ decreases with increasing temperature. Figure 13 shows a log–log plot of $\bar{r}_h$ vs. $\langle r_g^2\rangle_z^{1/2}$. At temperatures greater than the Θ temperature, the radius of gyration increases faster than the hydrodynamic radius, while below the Θ temperature the rates become comparable. Collapse of a polymer chain in poor solvent is not well understood, and only limited studies have been reported.[27] In our present investigation, we have experimental data on the contraction of the polymer coil below the Θ temperature. However, our results are not sufficient to denote a power law dependence even if it exists. Figure 14 shows a ln–ln plot of α_h vs. α_s, where we have included our results on the low molecular weight polystyrene (NBS 705 $M_w = 1.79 \times 10^5$) sample.[16] The solid lines represent the blob theory,[20,28] using eq 21 and 22,

$$\alpha_h(x) = \frac{4}{x^{1/2}}\left[2(3-x) + 3\left(\frac{x^{\nu-1}-1}{1-\nu} - \frac{x^{\nu-1}-x}{2-\nu}\right)\right]^{-1} \quad (21)$$

$$\alpha_s^2(x) = x^2(3-2x) + 6x^{1-2\nu}\left(\frac{1-x^{2\nu+1}}{2\nu+1} - \frac{1-x^{2(\nu+1)}}{2(\nu+1)}\right) \quad (22)$$

with $x \equiv N_\tau/N$ for $\nu = ^3/_5$ and 0.59, and the dot-dash line[29] denotes $\alpha_\eta^3 = \alpha_s^{2.43}$ with $\alpha_\eta^3 = \alpha_s^2\alpha_h$. Near the Θ temperature, our data appear to agree better with the Yamakawa theory. Again, the data below the Θ temperature are of interest as neither theory can be used to predict the

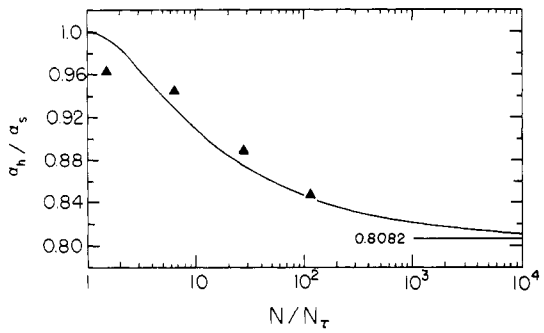

Figure 15. Plot of α_h/α_s as a function of N/N_τ. The solid line is the same as that in Figure 4 of ref 20.

collapse of polymer coils. At temperatures above the Θ temperature, we have plotted the temperature dependence of the ratio of the expansion factor of the hydrodynamic radius to the radius of gyration as shown in Figure 15. The solid line is represented by α_h/α_s using eq 21 and 22 with $\nu = {}^3/_5$.

Table II shows that for the high molecular weight polystyrene in *trans*-decalin the ratio of the hydrodynamic radius to the radius of gyration ($\bar{r}_h/\langle r_g^2\rangle_z^{1/2}$) is less than the theoretical value of 0.665 according to the Kirkwood-Reiseman theory,[29] and it becomes quite small at large temperature distances from the Θ temperature.

At finite concentrations, the frictional coefficient has the form

$$f = f^0(1 + k_f C + \ldots) \tag{23}$$

where $f^0 = 6\pi\eta_0 r_h$ and is related to D^0 by $D^0 = k_B T/f^0$. The hydrodynamic and thermodynamic factors are combined in k_D as[29]

$$k_D = 2A_2M - k_f - N_A V_1/M \tag{24}$$

where $\bar{v}$ ($=N_A V_1/M$) is the specific volume of the polymer with V_1 being the polymer molecular volume. Figure 16 shows the variation of k_D, k_f, and $M_w k_f/N_A\bar{V}_h$ with temperature, both below and above the Θ temperature. We note that there is a change of sign in k_D. The term $2A_2M$ has a dominating effect for high molecular weight polymer samples at temperatures away from the Θ temperature. The variation of $M_w k_f/N_A\bar{V}_h$ is governed mainly by the temperature dependence of k_f.

By dissolving a high molecular weight polymer sample (polystyrene, $M_w \sim 1.2 \times 10^7$) in a Θ solvent (*trans*-decalin), we have investigated the static and dynamical properties, in particular, the polymer dimensions in terms of the radius of gyration and the hydrodynamic radius in dilute solution, both above and below the Θ temperature. At temperatures above the Θ temperature, we present quantitative data under actual experimental conditions in the transition range before the parameters can be represented by their respective asymptotic power laws.

The blob theory[28] is in very good agreement with experiments at large values of N/N_τ where the asymptotic power laws are valid. In the transition region where the blob theory is expected to fail, the changes of the radius of gyration with respect to temperature and molecular weight follow closer to the gradual variation of the modified Flory theory. It is particularly important to note that power laws in nonasymptotic regions are not meaningful. Below the Θ temperature, a sharper contraction in both the radius of gyration and the hydrodynamic radius takes place. In particular, the hydrodynamic radius decreases in size about as fast as the radius of gyration, indicating no shape change over the few degrees in temperature below

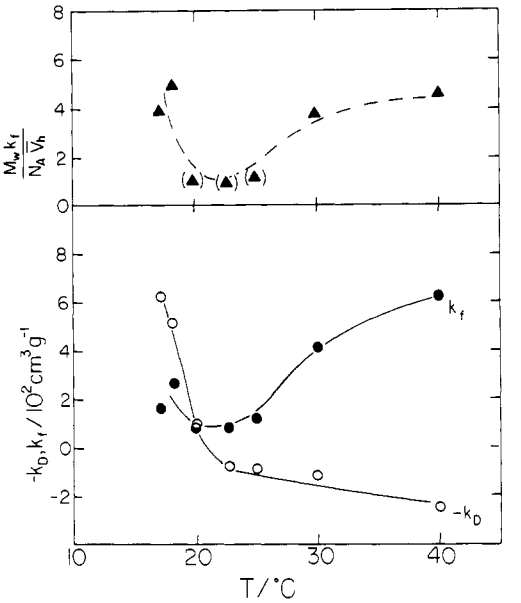

Figure 16. Variation of k_D, k_f, and $\bar{M}_w k_f/N_A\bar{V}_h$ with temperature. $\bar{V}_h$ ($=4\pi r_h^3/3$) is the hydrodynamic volume of the polymer molecule. We have used $\bar{M}_w = 1.34 \times 10^7$ in this computation.

the Θ temperature. The collapse of a polymer coil is a very interesting problem. Further studies are in progress.

References and Notes

(1) P. G. de Gennes, *Phys. Lett.*, *38A*, 399 (1972); *J. Phys. (Paris)*, **36**, L-55 (1975).
(2) J. des Cloizeaux, *J. Phys. (Paris)*, **36**, 281 (1975).
(3) M. Daoud, J. P. Cotton, B. Farnoux, G. Jannink, G. Sarma, H. Benoit, R. Duplessix, C. Picot, and P. G. de Gennes, *Macromolecules*, **8**, 804 (1975).
(4) M. Daoud and G. Jannink, *J. Phys. (Paris)*, **37**, 973 (1976).
(5) J. P. Cotton, M. Nierlich, F. Boue, M. Daoud, B. Farnoux, G. Jannink, R. Duplessix, and C. Picot, *J. Chem. Phys.*, **65**, 1101 (1976).
(6) P. G. de Gennes, *Macromolecules*, **9**, 587, 594 (1976).
(7) M. Daoud and P. G. de Gennes, *J. Phys. (Paris)*, **38**, 85 (1977).
(8) F. Brochard and P. G. de Gennes, *J. Chem. Phys.*, **67**, 52 (1977).
(9) M. Daoud and G. Jannink, *J. Phys. (Paris)*, **39**, 331 (1977).
(10) R. S. Adler and K. F. Freed, *J. Chem. Phys.*, **70**, 3119 (1979).
(11) M. Adam and M. Delsanti, *J. Phys. (Paris)*, **37**, 1045 (1976).
(12) M. Adam and M. Delsanti, *J. Phys. Lett. (Paris)*, **38**, L271 (1977).
(13) M. Adam and M. Delsanti, *Macromolecules*, **10**, 1229 (1977).
(14) B. Chu and T. Nose, *Macromolecules*, **12**, 347 (1979).
(15) T. Nose and B. Chu, *J. Chem. Phys.*, **70**, 5332 (1979).
(16) T. Nose and B. Chu, *Macromolecules*, **12**, 590, 599 (1979).
(17) Esin Gulari, Erdogan Gulari, Y. Tsunashima, and B. Chu, *J. Chem. Phys.*, **70**, 3965 (1979).
(18) B. Chu, Esin Gulari, and Erdogan Gulari, *Phys. Scr.*, **19**, 476 (1979).
(19) Erdogan Gulari, Esin Gulari, Y. Tsunashima, and B. Chu, *Polymer*, **20**, 347 (1979).
(20) A. Z. Akcasu and C. C. Han, *Macromolecules*, **12**, 276 (1979).
(21) J. des Cloizeaux, 7th Europhysics Conference on Macromolecular Physics, Strasburg, France, May 23–28, 1978.
(22) E. Dubois-Violette and P. G. de Gennes, *Physics*, **3**, 181 (1967).
(23) R. Kapral, D. Ng, and S. G. Whittington, *J. Chem.* Phys., **64**, 539 (1976).
(24) F. C. Chen, A. Yeh, and B. Chu, *J. Chem. Phys.*, **66**, 1290 (1977).
(25) Y. Tsunashima, K. Moro, and B. Chu, *Biopolymers*, **17**, 251 (1978).
(26) D. E. Koppel, *J. Chem. Phys.*, **57**, 4814 (1972).
(27) M. Nierlich, J. P. Cotton, and B. Farnoux, *J. Chem. Phys.*, **69**, 1379 (1978).
(28) G. Weill and J. des Cloizeaux, *J. Phys. (Paris)*, **40**, 99 (1979).
(29) H. Yamakawa, "Modern Theory of Polymer Solutions", Harper and Row, New York, 1971.
(30) H. Inagaki, H. Suzuki, M. Fujii, and T. Matsuo, *J. Phys. Chem.*, **70**, 1718 (1966).